[Article ID] 1003- 6326(2002)04- 0726- 08

Deformation of metallic glasses with special emphasis in supercooled liquid region ①

T. G. Nieh
(Lawrence Livermore National Laboratory, L-350, PO Box 808, Livermore, CA 94551, USA)

[Abstract] Upon deforming a metallic glass at low temperatures, shear tends to localize and this leads to a brittle behavior. However, in the high temperature, and particularly in the supercooled liquid region, homogeneous deformation begins to take place. A bulk amorphous Zr-10Al-5Ti-17.9Cu-14.6Ni alloy was observed to exhibit the Newtonian behavior at low strain rates but becomes non-Newtonian at high strain rates in the supercooled liquid region. Structures of the amorphous material, both before and after deformation, were examined using X-ray diffraction and high-resolution electron microscopy. Results showed the presence of nanocrystallites in the deformed samples. Thus, the non-Newtonian behavior is attributable to the concurrent crystallization of the amorphous structure during deformation. A mechanistic model is presented to interpret the observed non-Newtonian result. A phenomenological approach is also used to develop the deformation map for bulk metallic glasses in the supercooled liquid region.

[Key words] metallic glass; viscous flow; superplasticity; dynamic crystallization; amorphous alloys; Newtonian flow
[CLC number] TG 111.7; TG 139.8 [Document code] A

1 INTRODUCTION

Intensive efforts have been carried out over the past decade to develop means to slow down the phase transformation kinetics during the forming of metallic glasses. As a result of these efforts, some bulk metallic glasses (BMGs) can now be fabricated from the liquid state at cooling rates of about 1 ~ 10 K/s, which are close to those of conventional casting. This enables the production of BMGs with a thickness over 10 mm. While advances in amorphous metallic alloy development have been impressive, they have been made largely through empirical developments.

Bulk amorphous alloys have many potential applications resulting from their unique properties, such as superior strength and hardness[1, 2], excellent corrosion resistance[3], shaping and forming in a viscous state[4], reduced sliding friction and improved wear resistance[5], and low magnetic energy loss[6]. These properties should lead to applications in the fields of near-shape fabrication by injection molding and die casting, coatings, joining and bonding, biomedical implants, soft magnets for low energy loss, and synthesis of nanocrystalline and composite materials.

The mechanical behavior of BMGs can be classified by either inhomogeneous or homogeneous deformation. Inhomogeneous deformation usually occurs when a metallic glass is deformed at low temperatures (e.g. room temperature) and is characterized by the formation of localized shear bands, followed by rapid propagation of these bands, and catastrophic fracture. Consequently, when a metallic glass is deformed under tension it exhibits only limited macroscopic plasticity. Despite limited macroscopic plasticity, local strain within these shear bands can be sometimes quite significant. These bands are typically 20 ~ 30 nm in width and may be associated with crystallization[7] and even local melting[8]. Many different views exist on deformation mechanisms of inhomogeneous deformation in metallic glasses, and there is still no universal agreement.

Homogeneous deformation in metallic glasses usually takes place at high temperatures ($> 0.70T_g$, where T_g is the glass transition temperature), and the materials usually exhibit significant plasticity. The transition temperature from the inhomogeneous to homogeneous deformation (or brittle-to-ductile transition) is strongly dependent upon strain rate. For example, for the $Zr_{65}Al_{10}Ni_{10}Cu_{15}$ alloy, the transition temperature is about 533 K (corresponding to $0.82T_g$) at $5\times10^{-4}\ s^{-1}$, but it is 652 K (corresponding to $1.0T_g$) at $5\times10^{-2}\ s^{-1}$[9]. This rate dependence at the transition temperature suggests that homogeneous deformation is associated with some diffusional processes.

There is a growing interest in studying the homogeneous deformation of BMG, especially in the supercooled liquid region (SCL). This interest is, in part, stimulated by the fact that metallic glasses have excellent formability in this region, allowing net-shape forming. Several recent papers have been dedicated to the study of homogeneous deformation of BMG and a summary of some of the key observations is presented in Table 1.

It is noted that Kawamura et al[9] studied the high-temperature deformation of a $Zr_{65}Al_{10}Ni_{10}Cu_{15}$ metallic glass and found that, in the supercooled

① [Received date] 2001- 10- 08

Table 1 Deformation data of some metallic glasses in supercooled liquid region

Alloy	T_g, T_x/K	Strain rate/s^{-1}	m	Elongation	Ref.
$Pd_{78.1}Fe_{5.1}Si_{16}$	668, 683	~ 0.5	~ 1.0		[25]
$Co_{68}Fe_7Ni_{13}Si_7B_5$	836, 856	10^{-2}		180	[26]
$Ni_{77.5}Si_{7.5}B_{15}$			1.09		[27]
$La_{55}Al_{25}Ni_{20}$	480, 520	10^{-4}~ 1	1	1 800	[28]
$Zr_{65}Al_{10}Ni_{10}Cu_{15}$	652, 757	10^{-4}~ 10^{-1}	< 0.8	340	[12]
$Pd_{40}Ni_{40}P_{20}$	578, 651	10^{-4}~ 1	1.0		[12]
$Zr_{55}Al_{10}Ni_5Cu_{30}$	685, 763	< 10^{-4}	1.0		[13]
$Zr_{52.5}Al_{10}Ti_5Cu_{17.9}Ni_{14.6}$	631, 729	10^{-2}	~ 0.65	650	[23]

liquid region, plastic behavior was strongly dependent on strain rate. For each testing temperature, true Newtonian behavior was observed only in the low strain rate region. At high strain rates, the plastic flow became non-Newtonian, i.e. $m \neq 1$, in equation $\dot{\varepsilon} = K \cdot \sigma_m$, where m is the strain rate sensitivity exponent, $\dot{\varepsilon}$ is the strain rate, σ is the flow stress, and K is a constant. The specific strain rate at which the transition occurred depends upon the testing temperature. The authors argued that the non-Newtonian behavior is associated with stress overshoot at high strain rate (or high stress), and that the stress overshoot was caused by a change in atomic mobility because of rapid deformation-induced change of free volume. However, no experimental evidence, and in particular, no structural information, was presented.

The study of the plastic flow of another amorphous $Zr_{55}Al_{10}Ni_5Cu_{30}$ alloy in the supercooled liquid region also indicated a transition from Newtonian to non-Newtonian behavior as strain rate increased[10]. In this case, the authors invoked the absolute reaction rate theory to explain the observed increase in strain rate sensitivity with strain rate. However, it is pointed out that the absolute reaction rate theory is independent of the material structure, i.e., it does not include structure parameters.

In summary, the deformation behavior of BMGs in the supercooled liquid region can be Newtonian viscous flow or non-Newtonian, depending upon testing temperature and strain rate. Nonetheless, large tensile ductilities are universally obtained in BMG in the supercooled liquid region. In this paper, the authors offer another explanation for the observed non-Newtonian behavior from a structural point of view.

2 EXPERIMENTAL

The material used in the present study has a composition of Zr-10Al-5Ti-17.9Cu-14.6Ni. Zone-purified Zr bars (containing 1.23×10^{-5} O and 10^{-5} Hf, mole fraction), together with pure metal elements, were used as charge materials. The alloys were prepared by arc melting in inert gas, followed by drop casting into 6.4 mm-diameter by 7.2 cm-long Cu molds. The details of fabrication of the alloy have been described previously[8].

Tensile sheet specimens were fabricated from the as-cast material by means of electrical discharge machining. They had a gage length of 4.76 mm, a thickness of 1.27 mm and a width of 1.59 mm. Tensile tests were conducted using an Instron machine equipped with an air furnace. To minimize crystallization during testing a fast heating rate was used. Typically, the heating-plus-holding time prior to testing was about 25 min. For example, for a test at 410 ℃ at a constant strain rate of $10^{-2}\,s^{-1}$, the temperature profile was: 305 ℃ (5 min), 371 ℃ (10 min), 397 ℃ (15 min), 407 ℃ (20 min), 410 ℃ (23 min), and 410 ℃ (24 min). Constant strain rate tests were performed with a computer-controlled machine within a temperature range of 663 ~ 743 K at a constant strain rate of $10^{-2}\,s^{-1}$. To measure strain rate sensitivity exponents, both strain rate decrease and strain rate increase tests were performed.

X-ray diffraction was performed on undeformed and deformed specimens. These specimens were measured on the Unicat beamline 33-ID at the Advanced Photon Source, Argonne National Laboratory. The X-ray beam was focused to an ~ 0.2 mm × 0.1 mm spot. A slit was then placed in the beam to further reduce the beam size to 50 μm × 50 μm. The sample was placed on an x-y-z stage in the center of a six-circle Kappa diffractometer and oriented so that the surface of the sample was at small ~ 10° angle to the incident beam. The diffraction pattern was collected initially with a CCD camera that intercepted an ~ 30° × 30° fraction of solid angle. Measurements were made on all samples both near the fracture point and at various distances from the point.

Microstructural evolution in the deformed specimens was also examined using a high-resolution electron microscope (JEM-3000F model, operated at 300 kV). Areas near the grip and in the vicinity of the fracture tip of the tested specimens were examined.

For the grip area, the sample was mechanically thinned in water and, then, ion-milled using a liquid-nitrogen specimen cooling stage. For the areas near the tip of the fractured samples, on the other hand, TEM observations were directly carried out without additional thinning.

3 MECHANICAL PROPERTIES

The stress—strain behavior of the Zr-10Al-5Ti-17.9Cu-14.6Ni alloy at different temperatures at a strain rate of 10^{-2} s^{-1} is shown in Fig. 1. A yield drop (or stress overshoot) phenomenon is readily observed at low temperatures, and in particular at 663 and 683 K. For example, at 663 K the yield drop is 750 MPa (i.e. from 1 600 MPa to 850 MPa), which is about the same magnitude as its flow strength (~ 850 MPa). The yield drop phenomenon has also been reported previously in $Zr_{65}Al_{10}Ni_{10}Cu_{15}$[11] and $Zr_{55}Al_{10}Ni_5Cu_{30}$[10] in the supercooled liquid region. The yield drop was a result of rapid increase in free volume during high strain rate deformation[12]. Kawamura et al[11] demonstrated that the magnitude of yield drop depends on testing temperature and strain rate. Since the creation of excessive free volume and the subsequent annihilation are kinetic processes, it is not surprising that the yield drop is both temperature and rate dependent.

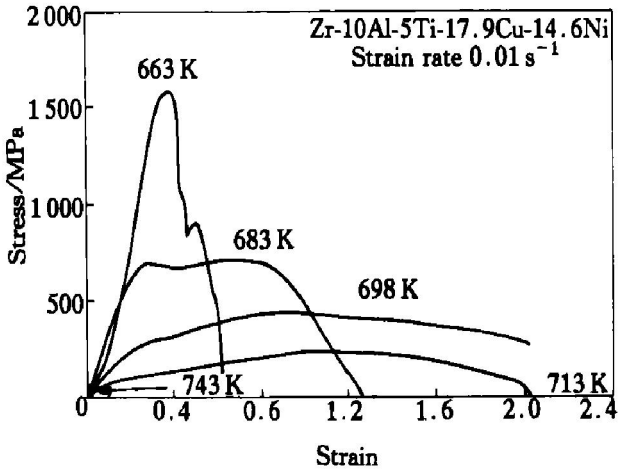

Fig. 1 Stress—strain curves of Zr-10Al-5Ti-17.9Cu-14.6Ni obtained at strain rate of 10^{-2} s^{-1} and temperatures within supercooled liquid region

The yield drop phenomenon disappears at high temperatures (> 683K), as shown in Fig. 1. At these temperatures, there is an initial hardening, followed by a gradual decrease in flow stress until final fracture. As shown in Fig. 1, the fracture strain increases with increasing test temperature and reaches a maximum value of about 2.0 (~ 650% elongation) at 698 and 713 K. At 743 K, which is above the crystallization temperature (729 K), the alloy becomes completely brittle. It is noted that samples which were deformed in the supercooled liquid region exhibit gradual necking. The final decrease in flow stress is, therefore, not a result of softening, but reduction in load bearing area. It is evident in Fig. 1 that both the flow stress and fracture strain are extremely sensitive to testing temperature. For example, with only a 15 K difference in testing temperature, the flow stress drops from 700 MPa at 683 K to about 400 MPa at 698 K, but the tensile elongation is almost tripled (230% to 630%). The flow stresses are noted to be relatively high; for example, at even 713 K the flow stress is about 200 MPa. This value is considerably higher than the flow stresses generally measured in metals or ceramics exhibiting superplasticity or extended ductility[13]. Flow stresses for superplastic metals or ceramics are typically lower than 35 MPa.

To characterize the deformation behavior, both strain rate decrease and increase tests were performed at 683 K. The results are presented as a logarithm stress—logarithm strain rate plot in Fig. 2. The value of strain rate sensitivity m is found to vary with strain rate. Specifically, the strain rate decrease test produces an m value close to unity in the low strain rate range ($< 10^{-3}$ s^{-1}). But, it decreases with increasing strain rate, and is much less than unity in the high strain rate range ($> 10^{-3}$ s^{-1}). In comparison, the strain rate increase test yields slightly higher flow stresses and m values. This may be caused by a temperature drift during the test. As noted previously, the flow stress is extremely sensitive to testing temperature. In summary, both strain rate change tests show that plastic flow is non-Newtonian in the high strain rate range.

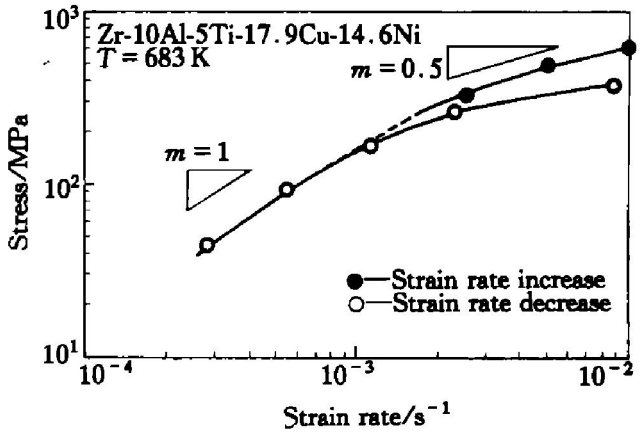

Fig. 2 Stress—strain rate relationship for Zr-10Al-5Ti-17.9Cu-14.6Ni at 683 K

4 STRUCTURAL ANALYSES

4.1 X-ray diffraction

X-ray diffraction was performed on three specimens: as-cast (undeformed), deformed at 713 K, and deformed at 683 K. The results are shown in Fig. 3. In the case of the 683 K specimen, an occasional sharp crystalline Debye ring was observed [as

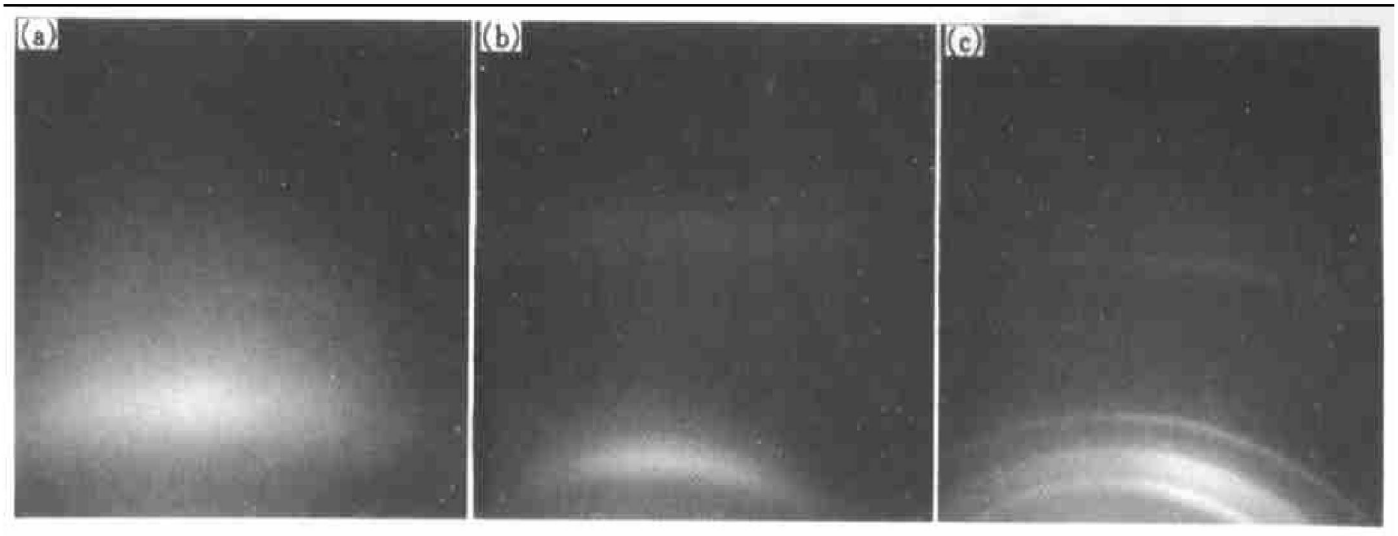

Fig. 3 X-ray diffraction pattern from as-cast (undeformed) (a), deformed at 683 K (b), and deformed at 713 K (c)
(Deformation strain rate 10^{-2} s^{-1})

shown in Fig. 3(b)], but did not appear to be correlated to the distance from the fracture tip. The crystalline size was estimated to be about 2.3 nm. In the case of the 713 K specimen, the sample was clearly more crystalline [as shown in Fig. 3(c)], and crystal pattern appeared very uniform. For the baseline comparison, measurements were also obtained from the as-cast sample. This sample showed a clearly amorphous pattern [as shwon in Fig. 3(a)] over the entire sample with an occasional sharp crystalline Debye Ring that is believed to be due to a thin oxide layer or some surface contaminant.

The CCD detector was then removed and replaced by an analyzer crystal to obtain high-resolution measurements of the Debye rings of the 713 K specimen. The crystalline phase was identified to be primarily Zr_2Ni. Crystalline grains are estimated to be at least as large as 9 nm. This observation is consistent with previous result[14]. The measurements show that the testing samples are undergoing a gradual amorphous to crystalline transformation uniformly as a function of processing temperature. These observations are also consistent with the fact that testing at 683 K produces better results; at 713 K significant crystallization occurred and led to embrittlement.

4.2 TEM observations

To further shed light on microstructural changes during deformation high-resolution electron microscopy (HREM) was employed to examine samples both before and after deformation. The microstructure of the as-cast sample is shown in Fig. 4. It is essentially featureless, although some local chemical ordering has been detected[15]. This amorphous structure is quite stable. For example, upon thermal exposure even at 683 K, which is slightly above the glass transition temperature, no microstructural change was discernible.

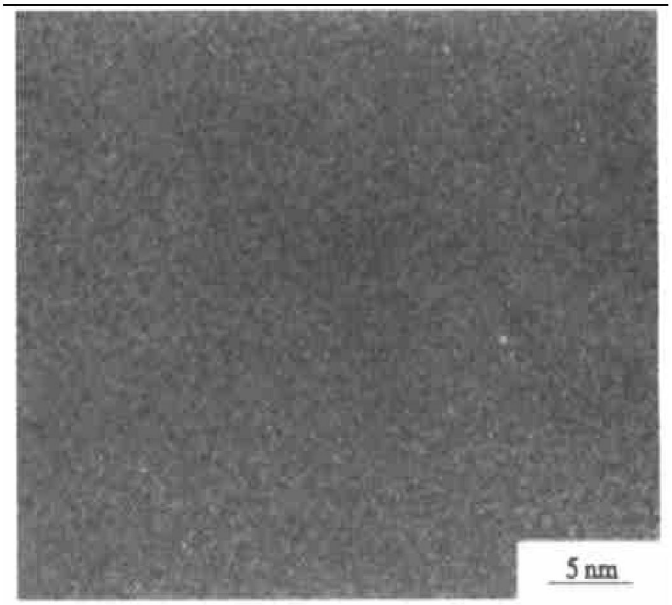

Fig. 4 Transmission electron micrograph showing amorphous nature of alloy in as-cast state

However, nanocrystallization was observed to occur at the region near the fracture tip of a sample tested at 683 K. A typical TEM image taken from the region is shown in Fig. 5(a). Figs. 5(b) and 5(c) are HREM images taken from the regions *A* and *B* in Fig. 5(a), respectively. The structure in Fig. 5(a) actually reveals two different morphologies. One morphology has an amorphous-like matrix but contains areas with local lattice fringes extending as small as 3 nm [as shown in Fig. 5(b)]. Another morphology is composed of an aggregate of nano-sized crystallites [as shown in Fig. 5(c)]. The sizes of these crystallites are as small as 5~10 nm, similar to the size estimated from the X-ray diffraction analysis. To investigate these crystallites, Fast Fourier Transformation (FFT) were performed. The patterns *i*, *j*, *k*, *l* in Fig. 5(d) are FFT from the encircled areas denoted *i*, *j*, *k*, *l* in Fig. 5(c), respectively. The relative orientations between these nanocrystallites are appar-

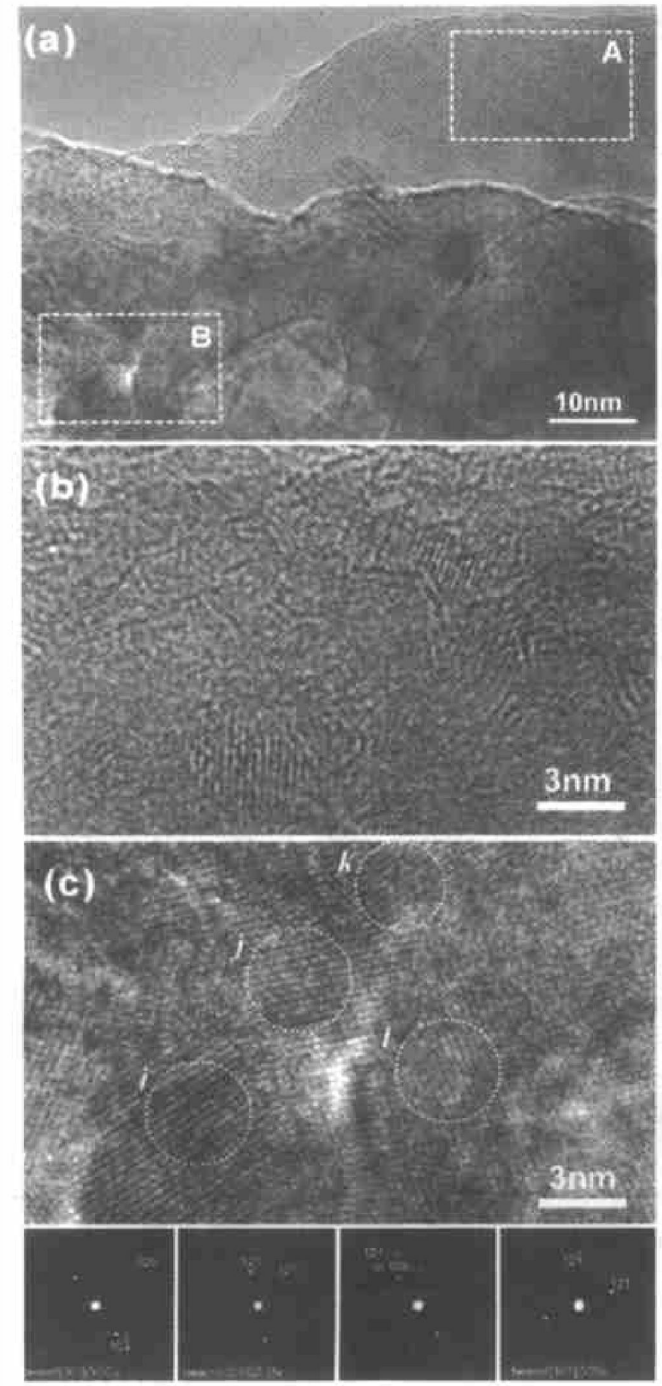

Fig. 5 Typical TEM image from fracture tip of amorphous Zr-10Al-5Ti-17.9Cu-14.6Ni sample deformed at 683 K at a strain rate of 10^{-2} s^{-1} (a), high magnification of area *A* (b), high magnification of area *B* (c), and SAED patterns from various regions in Fig. 5(c)

ently not low-angle. The Fourier transformed patterns can all be indexed by the structures of Zr_2Ni and Zr_2Cu.

The microstructure from the grip region of the sample deformed at 713 K shows finely dispersed nanocrystals dispersed in an amorphous matrix, as shown in Fig. 6. In the figure, a SAED pattern consisting of spotty diffraction rings with a diffuse background from the amorphous matrix is also included in the inset. The pattern indicates that the atomic planes in the nanocrystals embedded in the amorphous matrix are not greatly deformed.

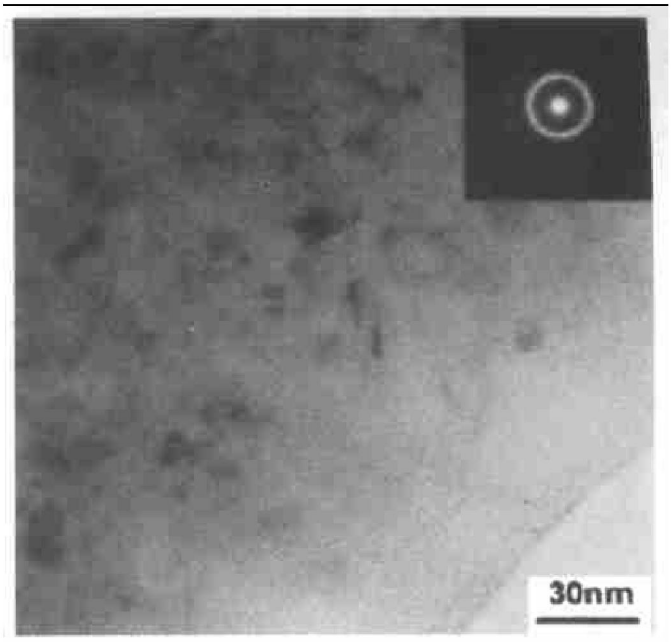

Fig. 6 TEM image from grip region of Zr-10Al-5Ti-17.9Cu-14.6Ni sample deformed at 713 K at a strain rate of 10^{-2} s^{-1}

5 DISCUSSION

The present study shows that the observed non-Newtonian behavior in the Zr-10Al-5Ti-17.9Cu-14.6Ni alloy at high strain rates is attributable to concurrent nanocrystallization during deformation. The presence of nanocrystallites in a metallic glass on the mechanical behavior is described as follows.

From a rheological viewpoint, the shear strain rate of a glass, $\dot{\gamma}$, is a nonlinear function of applied shear stress, τ, i.e.

$$\dot{\gamma} = f(\tau) \tag{1}$$

Assuming convergence, Eqn. (1) can be mathematically expanded into a Taylor series:

$$\dot{\gamma} = \sum_{i=1}^{n} A_i \tau^i = A_1\tau + A_2\tau^2 + A_3\tau^3 + A_4\tau^4 + A_5\tau^5 + \cdots\cdots \tag{2}$$

Each term in the above series has its own physical mechanism and can be identified with a specific, high-temperature, deformation process in polycrystalline solids. The first term ($A_1 \neq 0$) represents ideal Newtonian viscous flow. The second term ($A_2 \neq 0$) represents a grain-boundary sliding mechanism commonly observed in fine-grained, crystalline, superplastic materials. The third term ($A_3 \neq 0$) represents a deformation process controlled by viscous glide of dislocations in a crystalline lattice. The fourth term ($A_4 \neq 0$) represents a deformation process controlled by dislocation climb in a crystalline lattice. The non-zero values of the other $A_i\tau^i$ where $i > 5$ represent higher-order deformation mechanisms, such as the particle strengthening that is often observed in heavily-alloyed materials or structural composites.

In the case of an alloy which contains aggregates of nanocrystalline grains [as shown in Fig. 5(c)], to a first approximation the total deformation rate can be expressed by:

$$\dot{\gamma}_t = (1 - \varphi_c)\dot{\gamma}_a + \varphi_c \dot{\gamma}_c \quad (3)$$

where $\dot{\gamma}_t$ is the total strain rate, $\dot{\gamma}_a$ and $\dot{\gamma}_c$ are the strain rates resulting from the amorphous and crystalline phases, respectively, and φ_c is the volume fraction of the crystalline phase. Since the plastic flow of an amorphous alloy can be described by $\dot{\gamma}_a = A\tau$, and the plastic flow of a nanocrystalline, superplastic alloy can be described by $\dot{\gamma}_c = B\tau^2$, where τ is the flow stress, and A and B are material constants, Eqn. (3) becomes:

$$\dot{\gamma}_t = (1 - \varphi_c) A\tau + \varphi_c B\tau^2 \quad (4)$$

It is obvious from Eqn. (4) that the measured strain rate sensitivity would have to fall between 0.5, the value for grain boundary sliding in fine-grained crystalline material, and unity, the value for Newtonian viscous flow.

However, if an alloy contains isolated nanocrystalline grains in an amorphous matrix [as shown Fig. 5(b)], instead of having regions of nanocrystalline grains, the total deformation rate can now be expressed by:

$$\dot{\gamma}_t = (1 - \varphi_c) A\tau + \varphi_c B\tau^n \quad (5)$$

where $n > 5$, because the crystalline region of the material is treated as a dispersion strengthened solid. Obviously, the overall stress exponent for this alloy is also greater than unity, i.e. $m < 1$, but is not bounded at a lower level by $m = 0.5$ as in the case for the example of region of nanocrystalline grains.

Of additional interest is the drastic decrease in tensile elongation in BMG at temperatures immediately above the crystallization temperature. For instance, a $Zr_{52.5}Al_{10}Ti_5Cu_{17.9}Ni_{14.6}$ alloy (T_x = 729 K), when tested at 743 K (as shown in Fig. 1), exhibits practically zero ductility. This appears to be contrary to the conventional wisdom that a nano-grained alloy is expected to exhibit large elongations, presumably resulting from extensive grain boundary sliding. However, it must be pointed out that in the case of grain boundary sliding the sliding strain must be accommodated either by diffusional flow or by dislocation slip (e.g., climb or glide) across neighboring grains to prevent cavitation and fracture, as schematically illustrated in Fig. 7. Dislocation slip in a multi-component, ordered intermetallic compound is not expected to be easy even at temperatures near T_x (~ $0.8T_m$, where T_m is the melting point of the alloy).

On the other hand, when the grain size is sufficiently small, e.g. in the nanometer range, the diffusion distance that is required for accommodation is also short. (Diffusional distance is estimated to be of the same scale as the grain size.) In such a case, the possibility of diffusional accommodation must be also considered. The criterion for the prevalence of diffusional accommodation can be estimated using the equation:

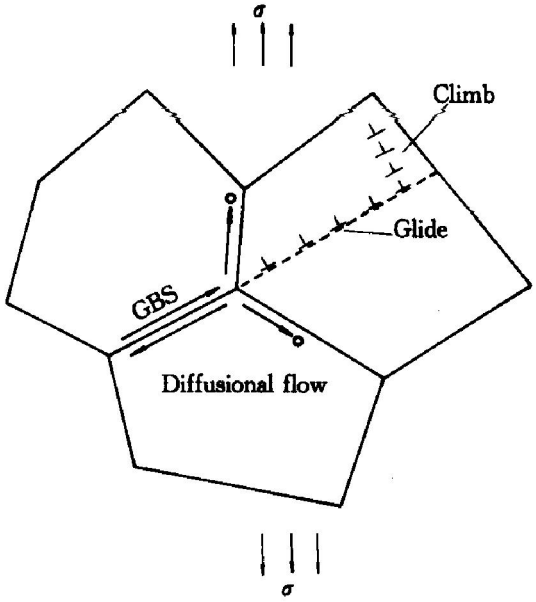

Fig. 7 Schematic of strain accommodation at grain triple junctions necessary to prevent cavitation

$$\sqrt{D_b t} > d \quad (6)$$

where D_b is the grain-boundary self diffusivity, t is the time, and d is the grain size. Obviously, this equation favors a small grain size, a slow strain rate, and fast diffusivity. If the diffusional process is not sufficiently fast to accommodate the sliding strain, especially at high strain rates, cavitation would take place and fracture follows. This accounts for the low tensile elongation in some metallic glasses even though they show a high m value at temperatures in the vicinity of T_x.

6 DEFORMATION MAP

As discussed above, nanocrystallization takes place in the present alloy during deformation in the supercooled liquid region, especially in the high strain rate range ($> 10^{-3}\ s^{-1}$). On the other hand, other studies[9, 12] suggested that the non-Newtonian behavior was associated with stress overshoot at high strain rate (or high stress), and the stress overshoot was caused by a change in atomic mobility due to rapid deformation-induced change of free volume. In principle, any of the relaxation or recovery process can be expressed as:

$$\text{Relaxation} \sim \exp(-Q_v/RT) \quad (7)$$

where Q_v, in this case, is the activation energy for the creation of free volume. The value of Q_v is probably similar to that for the diffusion of a volumetric defect in the amorphous alloy.

Spaepen[16] has proposed a conceptual strain rate—stress deformation map at room temperature for metallic glasses. In a similar manner, we can con-

struct a strain rate—temperature deformation map, plotted as a logarithmic strain rate versus the inverse of temperature plot shown schematically in Fig. 1. Within $T_g < T < T_x$, and assuming creation of free volume is the dominant mechanism, the Newtonian behavior is separated from non-Newtonian by the exponential function shown in Eqn. (7). When strain rate < $\exp(-Q_v/RT)$, Newtonian behavior is expected to prevail. Conversely, when strain rate > $\exp(-Q_v/RT)$, Newtonian flow dominates. The slope of the line separating the Newtonian and non-Newtonian regions gives the Q_v value. This division is qualitatively consistent with the observations of Kawamura et al[9, 17]. Namely, for the $Zr_{65}Al_{10}Ni_{10}Cu_{15}$ metallic glass, the activation energy Q of the stress relaxation decreased from (165 ±10) kJ/mol to (108 ±8) kJ/mol due to the yielding.

When the non-Newtonian flow is induced by nanocrystallization[10, 18], the situation is somewhat complex because nanocrystallization is not only a function of temperature but also stress (or strain)-dependent. However, nanocrystallization can still be written as another Arrhenius equation:

$$\text{Crystallization rate} \sim \exp[-(Q_c - \sigma\Omega)/RT] \quad (8)$$

where σ is the hydrostatic stress (or pressure, which is proportional to applied stress) and Ω the activation volume. The activation volume is expected to be slightly less than the size of short-range-ordered clusters. At room temperature, Ω is approximately the size of short-range-ordered clusters. In the supercooled liquid region, however, structural relaxation takes place and atoms are relatively mobile. The value of Q_c is expected to be higher than Q_v because free volume creation, unlike nanocrystallization, which requires both geometrical and chemical rearrangements, needs only short-range atomic diffusion. However, applied stress can aid to reduce the activation barrier for nanocrystallization[19~21].

Likewise, one can use Eqn. (8) to draw a line to divide the region into two. The slope of the line is $Q_c - \sigma\Omega$. Evidently, the exact location of the parting line is stress-dependent. An increase in stress (or strain rate) would cause a decrease in activation energy and, thus, accelerate nanocrystallization and promote non-Newtonian flow. This would widen the non-Newtonian region. At $T > T_x$, other mechanisms, e.g., grain-boundary sliding, begin to operate; materials behave in a non-Newtonian fashion. These results can be summarized in Table 2. It is noted that results from the present study and others[9, 10] indicate that a high strain rate and low temperature (i.e. near the glass transition temperature) condition favors non-Newtonian flow, which agree with Fig. 8 and Table 2.

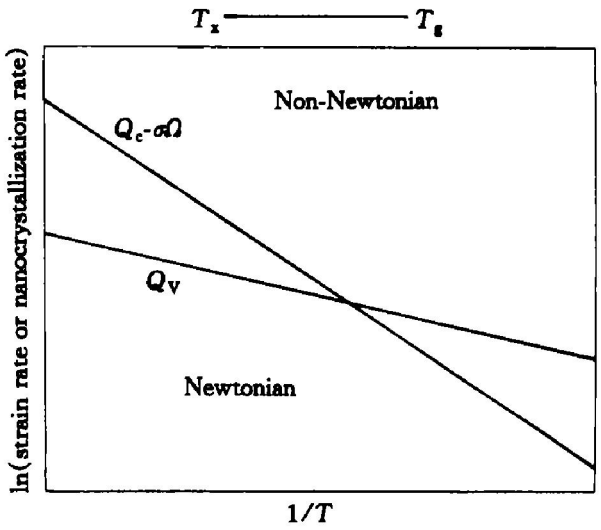

Fig. 8 Schematic deformation map for metallic glasses in supercooled liquid region

Table 2 Flow behavior in different temperature and strain rate regions

	High rate	Medium rate	Low rate
Low temperature ($T \sim T_g$)	Non-Newtonian	Non-Newtonian	Non-Newtonian
High temperature ($T \sim T_x$)	Newtonian	Mixed	Non-Newtonian

7 SUMMARY

Plastic flow of a bulk amorphous Zr-10Al-5Ti-17.9Cu-14.6Ni alloy was characterized in the supercooled liquid region. The alloy has excellent mechanical formability in the supercooled liquid region. The alloy exhibited Newtonian behavior at low strain rates, but became non-Newtonian as the strain rate increases. Microstructural examinations showed that even though tests were carried out in the supercooled liquid region, nanocrystallization still took place. Although the structure in the grip region remained amorphous nanocrystallization occurred in the deformed region, indicating that nanocrystallization was stress driven. Therefore, the observed non-Newtonian behavior can be attributed to glass instability during deformation. Composite models were presented to explain the strain rate sensitivity values. Multi-component BMG can be used as a precursor for nanocrystalline solids, however, nanocrystalline solids are not necessarily superplastic. The non-superplastic behavior is caused by the difficulty of strain accommodation at grain triple junctions.

ACKNOWLEDGMENT

This work was performed under the auspices of the U.S. Department of Energy (DOE) under contract No. W-7405-Eng-48 with Lawrence Livermore National Laboratory.

[REFERENCES]

[1] Inoue A, Kimura H M, Sasamori K, et al. Ultrahigh strength of rapidly solidified $Al_{96-x}Cr_3Ce_1Co_x$ (x = 1, 1.5 and 2%) alloys containing an icosahedral phase as a main component [J]. Mater Trans JIM, 1994, 35(2): 85– 94.

[2] Hays C C, Kim C P, Johnson W L. Microstructure controlled shear band pattern formation and enhanced plasticity of bulk metallic glasses containing in situ formed ductile phase dendrite dispersions [J]. Phys Rev Lett, 2000, 84(13): 2901– 2904.

[3] Hashimoto K. Current Topics in Amorphous Materials: Physics and Technology [R]. Sakurai Y, Hamakawa Y, Masumoto T, ed. Elsevier Science Publishers B. V., 1993. 167.

[4] Kawamura Y, Shibata T, Inoue A, et al. Deformation behavior of $Zr_{65}Al_{10}Ni_{10}Cu_{15}$ glassy alloy with wide supercooled liquid region [J]. Appl Phys Lett, 1996, 69(9): 1208– 1210.

[5] Wang J G, Choi B W, Nieh T G, et al. Nano-scratch behavior of a bulk Zr-10Al-5Ti-17.9Cu-14.6Ni amorphous alloys [J]. J Mater Res, 2000, 15(4): 913– 922.

[6] Inoue A, Miyauchi Y, Masumoto T. Soft magnetic Fe-Zr-Si-B alloys with nanocrystalline structure [J]. Mater Trans JIM, 1995, 36(5): 689– 692.

[7] Chen H, He Y, Shiflet G J, et al. Deformation-induced nanocrystal formation in shear bands of amorphous alloys [J]. Nature, 1994, 367(6463): 541– 543.

[8] Liu C T. Test environments and mechanical properties of Zr-base bulk amorphous alloys [J]. Metall Mater Trans A, 1998, 29A(7): 1811– 1820. [9] Kawamura Y, Nakamura T, Inoue A. Superplasticity in $Pd_{40}Ni_{40}P_{20}$ metallic glas [J]. Scr Mater, 1998, 39(3): 301– 306.

[10] Reger-Leonhard A, Heilmaier M, Eckert J. Newtonian flow of $Zr_{55}Cu_{30}Al_{10}Ni_5$ bulk metallic glassy alloys [J]. Scr Mater, 2000, 43: 459– 464.

[11] Kawamura Y, Shibata T, Inoue A, et al. stress overshoot in stress-strain curves of $Zr_{75}Al_{10}Cu_{15}$ metallic glass [J]. Mater Trans JIM, 1999, 40(4): 335– 342.

[12] Chen H S, Kato H, Inoue A. A fictive stress model and nonlinear viscoelastic behavior in metallic glasses [J]. Mater Trans JIM, 2001, 42(4): 597– 605.

[13] Nieh T G, Sherby O D, Wadsworth J. Superplasticity in Metals and Ceramics [M]. Cambridge University Press, Cambridge, UK, 1997.

[14] Wang J G, Choi B W, Nieh T G, et al. Crystallization and nanoindentation behavior of a bulk Zr-Al-Ti-Cu-Ni amorphous alloy [J]. J Mater Res, 2000, 15(3): 798– 807.

[15] Asoka-Kumar P, Hartley J, Howell R, et al. Chemical ordering around open-volume regions is bulk metallic glass $Zr_{52.5}Ti_5Al_{10}Cu_{17.9}Ni_{14.6}$ [J]. Appl Phys Lett, 2000, 77(13): 1973– 1975.

[16] Spaepen F. Microscopic mechanism for steady state inhomogeneous flow in metallic glasses [J]. Acta Metall, 1977, 25(4): 407– 415.

[17] Kawamura Y, Shibata T, Inoue A. Superplastic deformation of $Zr_{65}Al_{10}Ni_{10}Cu_{15}$ metallic glass [J]. Scr Mater, 1997, 37(4): 431– 436.

[18] Nieh T G, Mukai T, Liu C T, et al. Superplastic behavior of a Zr-10Al-5Ti-17.9Cu-14.6Ni metallic glass in the supercooled liquid region [J]. Scr Mater, 1999, 40(9): 1021– 1027.

[19] Homer C, Eberhardt A. Hot deformation of a metallic glass [J]. Scr Metall, 1980, 14: 1331– 1332.

[20] Csach K, Fursova Y V, Khonik V A, et al. Non-newtonian plastic flow a Ni-Si-B metallic glass at los streses [J]. Scr Mater, 1998, 39(10): 1377– 1382.

[21] Kawamura Y, Nakamura T, Inoue A, et al. High-strain-rate superplasticity due to Newtonian viscous flow in $La_{55}Al_{25}Ni_{20}$ metallic glass [J]. Mater Trans JIM, 1999, 40(8): 794– 803.

(Edited by YANG Bing)